*Desalination and Water Treatment*
www.deswater.com

doi: 10.5004/dwt.2017.20887

84 (2017) 153–159
July

# Enhanced photocatalytic activity of N-doped $TiO_2$ deposited on carbon fibers

Xili Shang[a], Zhenyu Li[b,*], Meiling Liu[b], Changhai Li[a,b,*]

[a]*Department of Chemical Engineering, Binzhou University, Binzhou 256603, China, Tel./Fax: +86 0543 3190097; emails: lichanghai2000@163.com (C. Li), xilishang@126.com (X. Shang)*
[b]*School of Chemical Engineering, Changchun University of Technology, Changchun 130012, China, emails: cclzy2001@163.com (Z. Li), liumlmail@163.com (M. Liu)*

Received 15 March 2016; Accepted 13 May 2017

**ABSTRACT**

N-doped $TiO_2$ were successfully deposited on the surface of carbon fibers (CFs) by the sol–gel method. The synthesized samples show much higher adsorption capacity and photocatalytic activity for the degradation of Rhodamine B than the pure $TiO_2$ under visible light irradiation. The doped N can further enhance the photocatalytic activity of $TiO_2$ due to the significant synergistic effect between $TiO_2$ and N, which can introduce intermediate level between the conduction band and valence band of $TiO_2$, thus decreasing the band gap values effectively. Moreover, the deposition of doped $TiO_2$ on CFs can promote the transfer and separation of photoproduction carriers, improving the adsorption capability of the catalyst and facilitating the recovery of catalyst. Meanwhile photocatalytic activity of the catalyst is reproducible which demonstrates excellent stability and recyclability factors, which are crucial for practical application.

*Keywords:* Doped; $TiO_2$; Carbon fiber; Photocatalytic

## 1. Introduction

Recently, semiconductor photocatalysis has received growing attention, as a green and advanced oxidation technology, and several different semiconductor photocatalysts have been extensively studied. Among these various semiconductor photocatalysts, $TiO_2$ has been widely applied owing to its strong photocatalytic ability, low cost and non-toxicity [1–3]. It is widely applied in pollutant treatment in gas and waste water, solar cells, self-cleaning surfaces, hydrogen decomposition from water [4–6]. However, there are some drawbacks to limit its practical application. For example, pure $TiO_2$ can only be excited by the UV light due to its wide intrinsic band gap [7–9]. Therefore, various approaches have been studied to improve the performance of $TiO_2$ photocatalytic, such as ions doping, dye sensitization, noble metal loading and semiconductor compound. The doping of various elements into $TiO_2$ is an effective method to improve the photocatalytic activity since the recombination of photogenerated electrons and holes can be hindered [10–12]. For example, Asahi et al. [13] and Tong et al. [14] doped N and $Fe^{3+}$ into $TiO_2$ catalysts, respectively, to improve the visible light catalysis activity of the $TiO_2$. The $TiO_2$ crystal lattice can be distorted with the introduction of impurity atoms, which can promote the transfer and separation of photoproduction carriers. A large amount of impurity level were formed between the conduction band (CB) and valence band (VB) of $TiO_2$ with the atomic orbital coupling hybrid of N, Ti and O, by which the band gap values of the catalyst can be decreased effectively. Therefore, photocatalytic activity of catalyst can be also improved.

On the other hand, the adsorption performance of the catalytic material can affect the degradation effect, the adsorption process could increase the encounter probability between the pollutants and catalysts as the pollutants are degraded by catalysis [15,16]. Furthermore, the separation and recovery of $TiO_2$ photocatalysts from the treated water is another important problem for industrial applications [17,18]. Much research

* Corresponding author.

is focused on loading $TiO_2$ onto such porous materials, such as silica, zeolites, and activated carbon [19]. The porous materials usually have good pollutant adsorption and can promote photocatalytic efficiency. There are various support materials such as activated carbon, molecular sieve, clay, and silica gel. Carbon fiber (CF) is widely used as a support in various applications because of its uniform pore structure, extensive pore surface area, and high adsorption ability [20–22]. $TiO_2$ and activated carbon fiber (ACF) composite photocatalytic materials ($TiO_2$/ACF) and founded that the methyl orange could be removed rapidly with those samples under UV irradiation. Yao and Shi [24] synthesized $TiO_2$/ACF by a hydrothermal method and study of its adsorption property. It was reported that the Rhodamine B (RhB) molecules are more easily adsorbed on a polar surface because of their cationic nature; in addition, the nanoparticles adsorption effect of immobilized $TiO_2$ helps to promote the adsorption of RhB molecules. Thus, these results reveal enhanced adsorption ability for the $TiO_2$/ACF composite fiber. Liu et al. [25] prepared (Fe, N) co-doped $TiO_2$ powders by hydrothermal synthesis and found that doped titanium dioxide powders had excellent photocatalytic activity during the process of photodegradation of formaldehyde and total volatile organic compound gases under visible light irradiation. The Fe and N doping induced the formation of new states closed to the VB and CB, respectively. The co-operation of the N ion leads to the much narrowing of the band gap and greatly improves the photocatalytic activity in the visible light region [26,27]. Meanwhile, the co-doping can also promote the separation of the photogenerated electrons and holes [28].

In this paper, CFs deposited with N-doped $TiO_2$ composite (NTCF) were synthesized by the sol–gel method, in which the costless ferric nitrate and urea were used as the iron and nitrogen source, respectively. The adsorption properties and photocatalytic performances of the material under visible light irradiation were investigated by using RhB as a target compound. The as-prepared materials exhibit higher photocatalytic activity than pure $TiO_2$ (P25) under visible light irradiation, due to the doping N can decrease the band gap and promote the separation of the photon-generated carrier. It also has been proved that the photocatalytic activities of NTCF are stable and durable by the cycle photocatalytic test. In this study, an efficient photocatalytic material was prepared by simple method and inexpensive raw materials, which was very necessary for large-scale applications.

## 2. Experimental

### 2.1. Materials

CFs was purchased from the Japanese Toray Engineering (T700SC-12000-50C, Tokyo, Japan). Tetrabutyl titanate (TBOT), acetic acid, ethanol absolute (EtOH), acetone, urea and RhB were purchased from the Sinopharm Chemical Reagent Corporation (Shanghai, China). Pure $TiO_2$ (Degussa P25) was employed as a reference photocatalyst. All chemicals were of analytical grade and were used without further purification.

### 2.2. Sol–gel process of NTCF

A series of N–$TiO_2$ composites were prepared by a sol–gel method. First, TBOT (18.8 mL) was added into EtOH (31.2 mL) and kept stirring for 30 min, then a certain amount of urea were added directly to the initial TBOT solution with the acetic acid. A homogeneous solution (solution A) was obtained after continuous stirring for 1 h. Acetic acid (5.0 mL) and EtOH (6.2 mL) were added into distilled water (3 mL) with stirring to form a homogeneous solution (solution B). Solution B dripped into solution A slowly in 60 min and kept stirring for 3 h and the N–$TiO_2$ sol was obtained. The pretreated CFs dipped in the N–$TiO_2$ sol repeatedly for 35 min, then pulled out slowly and dried in a vacuum oven at 60° for 8 h, followed by calcined at 500°C for 4 h in air to obtain the NTCF photocatalyst.

### 2.3. Characterization

The morphology of NTCF was observed on an SU-70 scanning electron microscope (Hitachi Limited, Japan). The X-ray diffraction pattern was obtained with a D8 Advance diffractometer (Bruker AXS, Germany) using Cu K$\alpha$ radiation at a tube voltage of 50 kV and tube current of 100 mA. Fourier-transform infrared spectroscopy (FTIR) analyses were performed on a FTIR spectrometer (PerkinElmer, USA) using samples dispersed in anhydrous KBr. The UV-visible diffuse reflectance spectrum (UV--Vis DRS) data of grinded solid powders (sample + KBr) was recorded on a UV-3600 spectrophotometer (Shimadzu, Japan) at room temperature using $BaSO_4$ as reference material. The chemical composition of the samples was analyzed using Thermo Escalab 250Xi X-ray photoelectron spectrometer (Thermo Electron Corporation, USA). The nitrogen adsorption–desorption isotherm was measured using Tristar II 3020 (Micromeritics Instrument Corporation, USA).

### 2.4. Photocatalytic experiments

The photocatalytic experiments were carried out in a XPA-7 photoreactor (Xujiang Electromechanical Plant, Nanjing, China) equipped with a 500 W high-pressure xenon lamp as the visible light source. First, 0.0325 g of as-synthesized catalyst was added to quartz tube with a solution of RhB (70 mL, $2.0 \times 10^{-5}$ mol·L$^{-1}$). Then, the tube was mounted onto the rotating disk inside the photoreactor and kept in dark for 30 min to reach absorption equilibrium. Afterwards, the tube was exposed to light with continuous purging of air to provide oxygen. A certain amount of suspensions were extracted at regular intervals and centrifuged to separate the supernatant liquid. The supernatant liquid was collected and analyzed by a UV–Vis spectrometer to measure the temporal changes of solution concentration.

The degradation efficiency (%) was calculated as follows:

$$\text{Degradation (\%)} = (C_0 - C)/C_0 \times 100\% \quad (1)$$

where $C_0$ is the initial RhB concentration and $C$ is the residual RhB concentration.

## 3. Results and discussion

### 3.1. Morphology and structure of NTCF

The morphologies of the catalysts are presented in Fig. 1. The surface of CFs is smooth and has a large amount of long

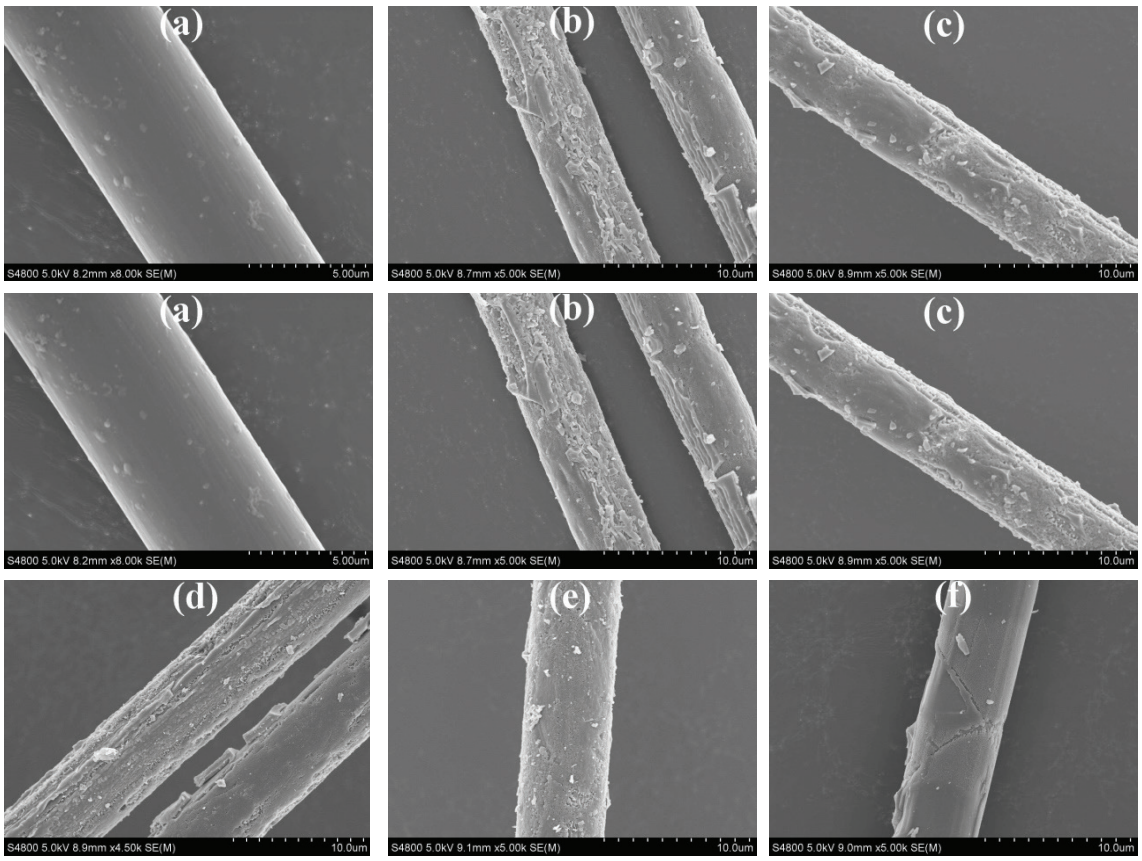


Fig. 1. SEM images. (a) Pure CFs; (b–f) NTCF with different loading: (b) *n*(N:Ti) = 0.4%:1, (c) *n*(N:Ti) = 0.8%:1, (d) *n*(N:Ti) = 1.6%:1, (e) *n*(N:Ti) = 3.2%:1 and (f) *n*(N:Ti) = 4.8%:1.

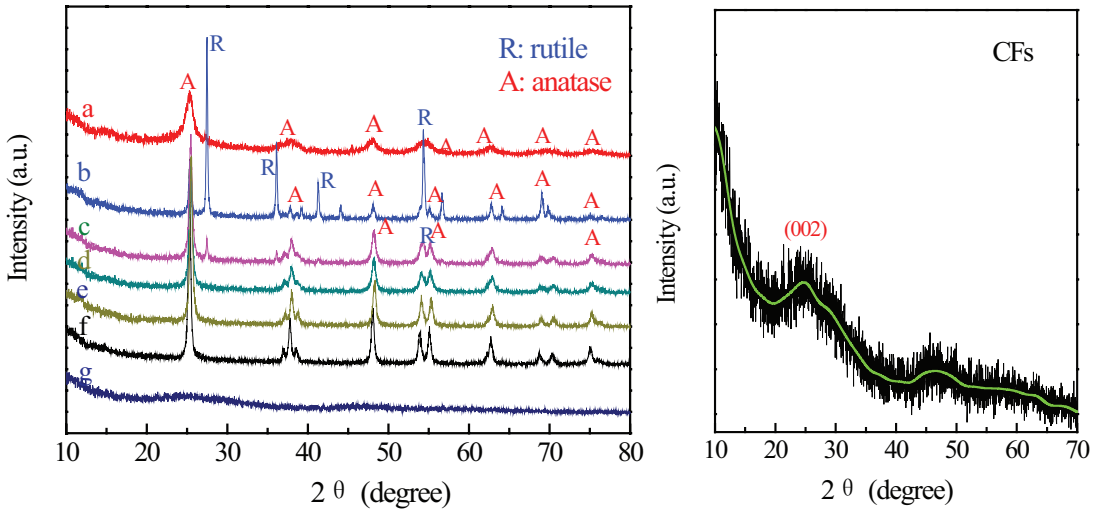


Fig. 2. XRD patterns of $TiO_2$ (a) and NTCF: (b) *n*(N:Ti) = 0.4%:1, (c) *n*(N:Ti) = 0.8%:1, (d) *n*(N:Ti) = 1.6%:1, (e) *n*(N:Ti) = 3.2%:1, (f) *n*(N:Ti) = 4.8%:1 and (g) CFs.

and shallow grooves as is benefited for surface adsorption of target pollutant as shown in Fig. 1(a). Figs. 1(b)–(f) show scanning electron microscope (SEM) images of NTCF prepared with different N loading. Compared with the pure CFs, the N–$TiO_2$ nanoparticles are deposited on the surface of CFs with favorable dispersibility, and the loading amounts of N/$TiO_2$ increase as the ratio of N increases from 0.4% to 4.8%. As can be seen in Figs. 1(b) and (c), cracks appeared on the

NTCFs surface and N–$TiO_2$ nanoparticles separated from the CFs, which may be caused by high temperature annealing and the little load volumes of N–$TiO_2$ with uneven distribution. When the content of N reached up to 4.8% (Fig. 1(f)), the deposition amount of immobilized N–$TiO_2$ apparently achieved to maximum and the surface of NTCF was smooth and uniform.

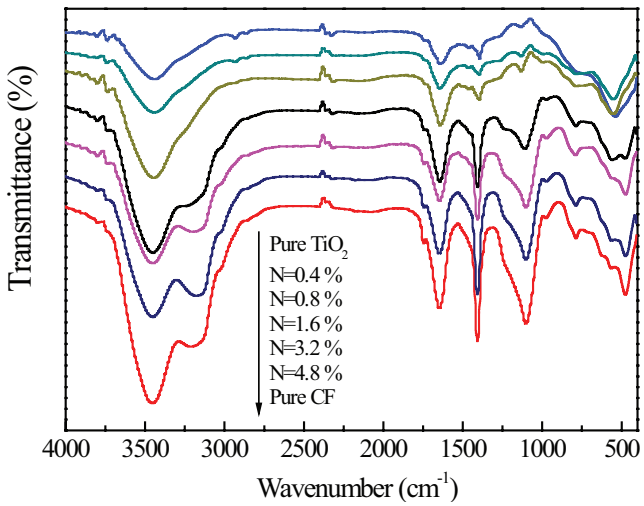


Fig. 3. FTIR spectra of NTCF.

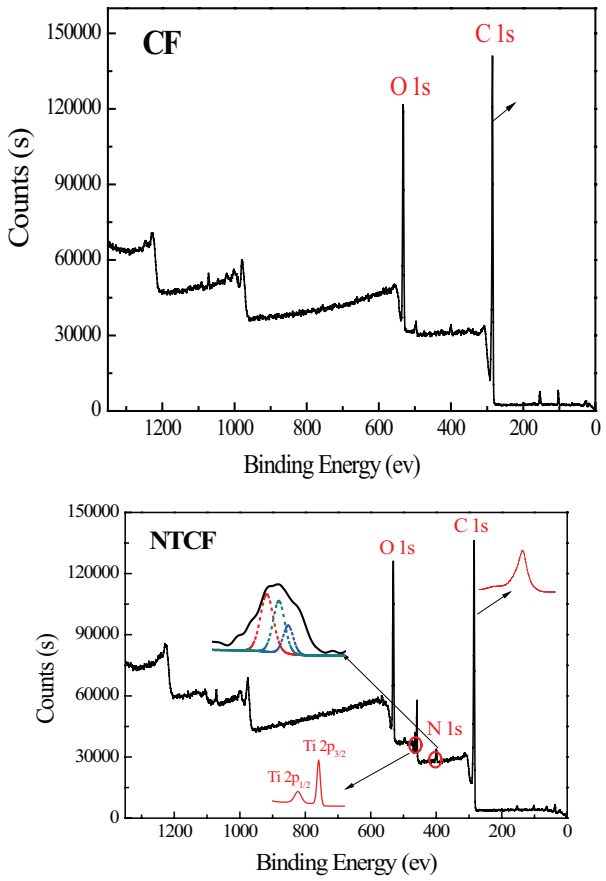


Fig. 4. The XPS spectra of CFs and NTCF.

Fig. 2 shows the X-ray diffraction (XRD) patterns of the synthesized samples. The original $TiO_2$ exhibits typical patterns that can be well indexed to the phases of anatase and rutile. The characteristic diffraction peaks at 2θ values of 25.3°, 37.9°, 48.4°, 53.9°, 55.1°, 62.8°, 68.8°, 70.3° and 75.0° correspond to the crystal planes of (101), (004), (200), (105), (211), (204), (116), (220) and (215) of the anatase phase $TiO_2$ (JCPDS No. 21-1272). In addition, the rutile phases have diffraction peaks with 2θ values of 27.4°, 36.1°, 41.2° and 56.7° corresponding to rutile (110), (101), (111) and (220) crystal planes, respectively. The structure of the $TiO_2$ in the prepared composite is also identified as rutile and anatase obviously that is very similar to the pure $TiO_2$.

The FTIR spectra of CFs and NTCF are shown in Fig. 3. It is believed that the band at 400–850 $cm^{-1}$ corresponds to the Ti–O–Ti stretching vibration in crystal $TiO_2$ [29], indicating that the molecular structure of $TiO_2$ was not changed in the process of heat treatment, which is consistent with XRD results. Another peak centered at around 1,348 $cm^{-1}$ is consistent with the C=C and C–C stretching bands of the carbon. The broad peak at 3,400 and 1,630 $cm^{-1}$ are assigned to the surface adsorbed water and hydroxyl groups.

In order to study the relation between N/$TiO_2$ and CFs, ultrasonic cleaning tests were carried out for NTCF samples (the doping ratio of $n$(N:Ti) = 4.8%:1). The CFs and NTCF were studied using X-ray photoelectron spectroscopy (XPS)

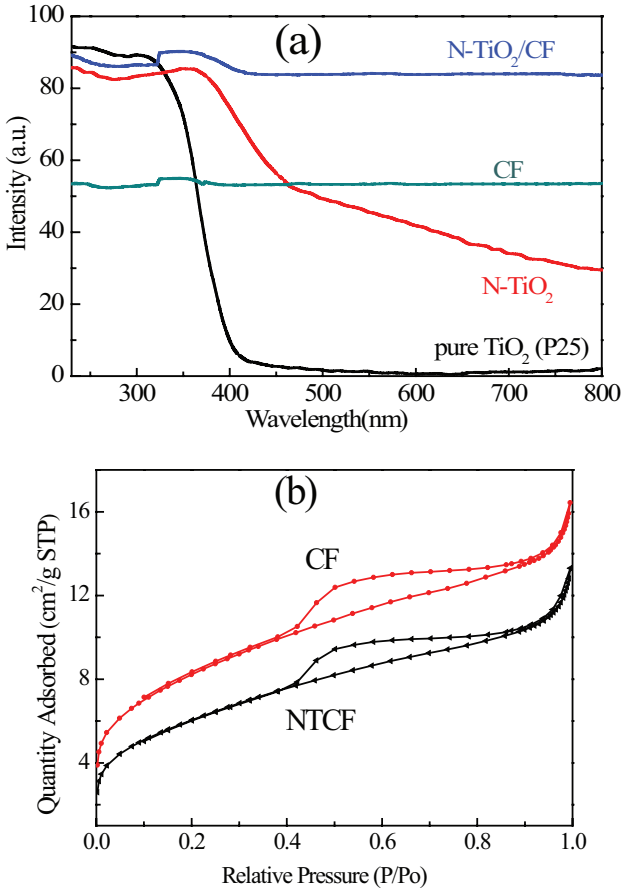


Fig. 5. (a) UV–Vis DRS of the as-prepared samples and (b) $N_2$ adsorption and desorption isotherms of pure CFs and NTCF.

measurements after ultrasonic cleaning. Fig. 4 shows the XPS spectra of the CFs and N/$TiO_2$ sample. In Fig. 4, the peaks of 456.48 and 462.28 eV correspond to the peaks of Ti $2p_{3/2}$ and Ti $2p_{1/2}$, respectively, which is consistent with the theoretical value of $Ti^{4+}$ in the $TiO_2$ in documents mentioned [30]. In addition, XPS data have detected the existence of C=NH, C–N and C–$N^+$ correspond to 398.9, 400.3 and 401.5 eV, respectively, which prove a good combination between the N–$TiO_2$ and the CFs. And this is benefit for the stability of the catalysts.

The photocatalytic activity of the material is related to its light absorption performance. The optical properties of the samples were investigated using the UV–Vis diffuse reflectance spectra as shown in Fig. 5(a). For comparison, pure $TiO_2$ (P25), CFs and doped $TiO_2$ were also evaluated. Pure $TiO_2$ have no response to visible light, however, the optical absorption edge is shifted to visible light region after modified by doping with N as is in consistent with the literature reported [31]. NTCF has a strong light absorption performance in both ultraviolet and visible region as shown in Fig. 5(a) which is similar to the CFs, which is attributed to the enhanced optical absorption properties of CFs compared with that of the pure $TiO_2$. The broad absorption of NTCF is expected to improve its photocatalytic activity in the visible region.

The specific surface area, pore diameter and pore volume of CFs and NTCF were measured by $N_2$ adsorption–desorption technology. Fig. 5(b) shows the adsorption isotherm, and Table 1 lists the detailed data of surface area, pore diameter and pore volume of the CFs and NTCF. Specific surface area of the CFs and NTCF was 28.04 and 20.86 $m^2 \cdot g^{-1}$, pore volume was 0.025 and 0.021 $cm^3 \cdot g^{-1}$ by calculating on the adsorption branch, pore size was 35.31 and 38.31 nm, respectively. The $N_2$ adsorption–desorption test results show that the specific surface area of NTCF decreases, while the pore size is increased, this may be that the catalyst has certain degree of coalescence in the process of heat treatment [32].

Table 1
Structural characteristics of catalyst

| | Surface area ($m^2 \cdot g^{-1}$) | Pore volume ($cm^3 \cdot g^{-1}$) | Pore size (nm) |
|---|---|---|---|
| CFs | 28.04 | 0.025 | 35.31 |
| NTCF | 20.86 | 0.021 | 38.31 |

### 3.2. Photocatalytic test

The photocatalysis performance of the materials was evaluated with RhB as the target pollutants with initial concentration of $2.0 \times 10^{-5}$ mol·$L^{-1}$ under visible light irradiation in 80 min. The results of photocatalytic degradation of RhB for composite fibers irradiated under visible light are shown in Figs. 6(a) and (b). The RhB could hardly be degraded

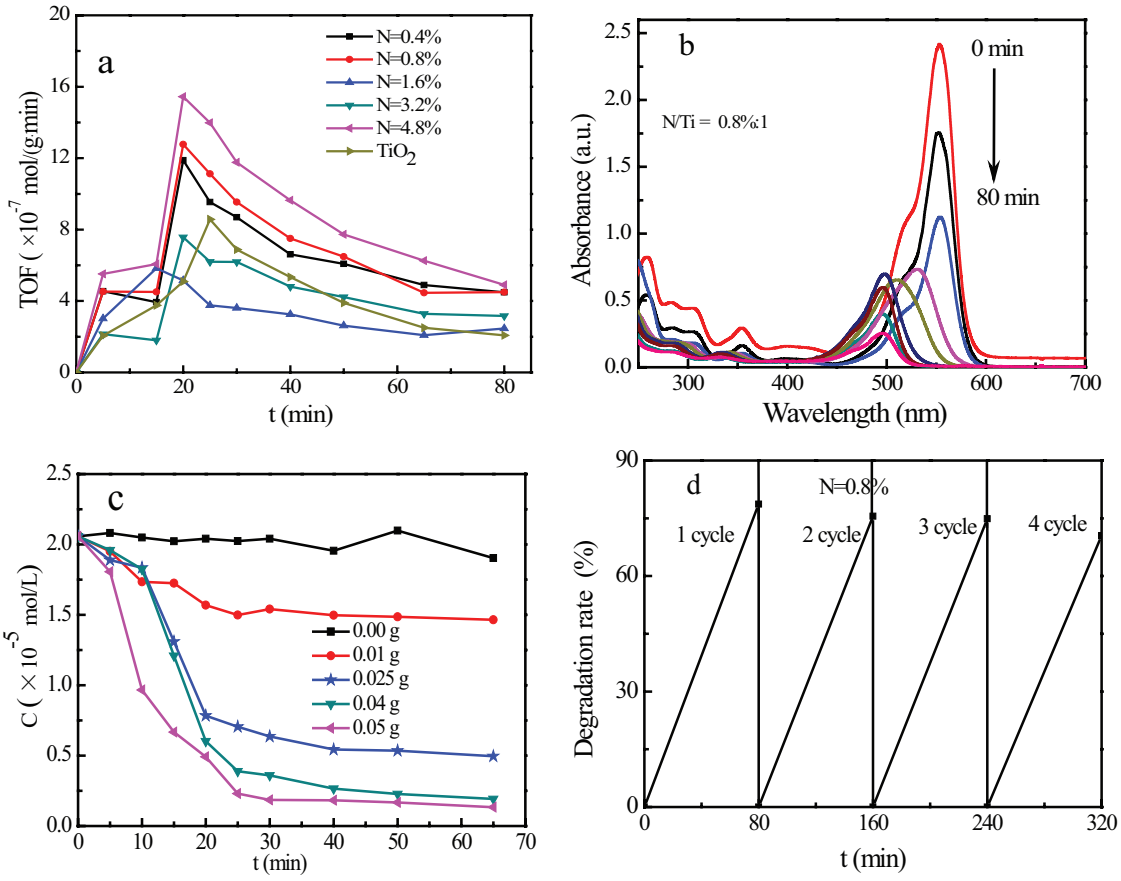


Fig. 6. Photocatalytic activity of the as-synthesized samples. (a) The TOF of RhB. (b) UV–Vis spectral changes of RhB. (c) The effects of the dosage of catalyst. (d) Recycling properties of NTCF.

under visible light irradiation. Thus, the removal of RhB is owing to the adsorption and photocatalytic degradation. In heterogeneous catalytic reaction, turnover frequency (TOF) is the number moles of conversion reactants on unit mass catalyst in unit time. The concentration of RhB reduced rapidly in the dark, as was due to the excellent adsorption abilities of the composite. The optimal *n*(N/Ti) ratio was 0.8%:1, in which rate the composites showed good photocatalysis activity exposed to visible light (Fig. 6(a)). It can be seen that the loaded amount of NTCF has a significant effect on the photocatalytic activity of the composite fibers. The concentration of the adopted pollutant (RhB) almost no change after irradiation of 80 min under the visible light when absence of a catalyst. The degradation rate did not increase with the increase of dosage of catalyst instead reduce, which may be caused by the block of the transmission of the incoming light as high concentration of the catalyst was used. To explore the stability and continuous photocatalytic activity of NTCF, recycling experiments were also conducted under the same reaction conditions. The catalyst was collected and washed with deionized water to remove the bulk solution, dried in oven at 90°C for 0.5 h, and then the renewed NTCF was used directly in the next run. As shown in Fig. 6(d), there is no appreciable loss of photocatalytic activity observed when the photocatalyst was used four times. The possible reason is that the separation of $e^-$ and $h^+$ was promoted by the introduction of impurity elements, which can increase the crystal lattice distortion of $TiO_2$. On the other hand, a large amount of impurity level formed between the CB and VB of $TiO_2$ with the atomic orbital hybridization of N, Ti and O [33,34], so the band gap of the composite was decreased than that of the pure $TiO_2$, and the visible light can also stimulate the transition of the photogenerated charge carriers.

### 3.3. Proposed mechanism

Combining with the results of the morphology, structure and photocatalytic test, we know that N and CFs played an important role in photocatalytic RhB degradation system.

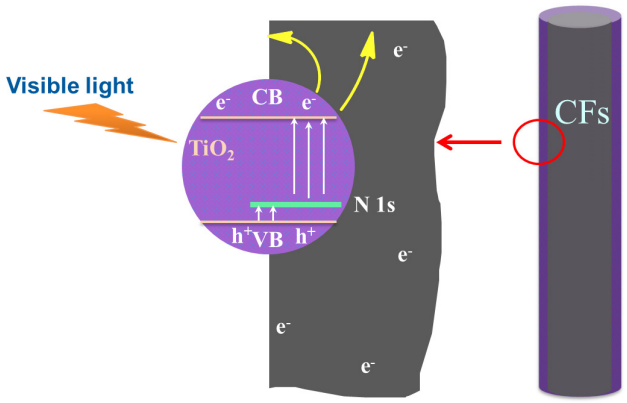


Fig. 7. The schematic diagram of possible electron–hole separation and transport at the interface of NTCF composite.

The formation mechanism of NTCF can be deduced in Fig. 7. The electron cannot be excited from the VB to the CB for the pure $TiO_2$ under visible light. For NTCF samples, the band gap of $TiO_2$ is narrowed due to the replacement of the lattice oxygen by nitrogen, resulting in the formation of O–Ti–N bonds and facilitating to extend the adsorption region from the UV to the visible light [35]. As a result, the electron can be excited in smaller gap [36]. In addition, after high temperature calcinations, C=NH, C–N and C–$N^+$ were formed between N and CFs which effectively transfer electronic through the interface with N-doped $TiO_2$ nanoparticles.

## 4. Conclusion

In this paper, we have successfully synthesized Fe, N co-doped $TiO_2$ deposited on carbon fibers (NTCF) which was characterized by XRD, SEM, XPS, FTIR, UV–Vis DRS and $N_2$ adsorption–desorption measurements. The N–$TiO_2$ nanoparticles are loaded with good dispersity on the surface of CFs. The as-prepared composites exhibited an enhanced adsorption property and photocatalytic activity for the removal of RhB than that of pure $TiO_2$ (P25), and the doping contents significantly affect the photocatalytic efficiency, the degradation rates of RhB increased from 33.8% to 78.6% as the ratio of N varied from 0.4% to 4.8%. The doping of N induced a red-shift of the absorption curves due to the inclusion of new intragap energy levels. On the other hand, the deposition on CFs benefits the adsorptive function of the composites for the organic pollutants and the effective separation of electron and hole. By which an efficient visible light response and photogenerated charge carriers separation system was been established for the removal of pollutants via adsorption–photocatalysis processes.

## Acknowledgments

This work was partially supported by the Shandong Provincial Natural Science Foundation, China (ZR2015BL016), Key research and development Plan Project of Shandong Province, China (2017GGX80104),National Natural Science Foundation of China (21507006), and Key Science and Technology Program of Jinlin Province, China (20130206069SF).

## References

[1] J. Matos, J. Laine, J.M. Herrman, Synergy effect in the photocatalytic degradation of phenol on a suspended mixture of titania and activated carbon, Appl. Catal., B, 18 (1998) 281–291.
[2] S.X. Liu, Z.P. Qu, X.W. Han, C.L. Sun, A mechanism for enhanced photocatalytic activity of silver-loaded titanium dioxide, Catal. Today, 93 (2004) 877–884.
[3] L.H. Keith, W.A. Telliand, ES&T special report: priority pollutants. I. A perspective view, Environ. Sci. Technol., 13 (1979) 416–423.
[4] M. Machida, B. Fotoohi, Y. Amamo, H. Kanoh, L. Mercier, Cadmium(II) and lead(II) adsorption onto hetero-atom functional mesoporous silica and activated carbon, Appl. Surf. Sci., 258 (2012) 7389–7395.
[5] Z. Wu, Z. Cheng, W. Ma, Adsorption of Pb(II) from glucose solution on thiol-functionalized cellulosic biomass, Bioresour. Technol., 104 (2012) 807–809.
[6] H.J. Zhang, G.H. Chen, D.W. Bahnemann, Photoelectrocatalytic materials for environmental applications, J. Mater. Chem., 19 (2009) 5089–5121.

[7] M.R. Hoffmann, S.T. Martin, W.Y. Choi, D.W. Bahnemann, Environmental application of semiconductor photocatalysis, Chem. Rev., 95 (1995) 69–96.
[8] X. Wang, X.J. Wang, J.F. Zhao, Bioframe synthesis of NF-$TiO_2$/straw charcoal composites for enhanced adsorption-visible light photocatalytic degrade RhB, RSC Adv., 21 (2015) 12233–12240.
[9] I.M. Arabatzis, T. Stergiopoulos, M.C. Bernard, Silver-modified titanium dioxide thin films for efficient photodegradation of methyl orange, Appl. Catal., B, 42 (2003) 187–201.
[10] I.H. Tseng, J.C.S. Wu, H.Y. Chou, Effects of sol-gel procedures on the photocatalysis of Cu/$TiO_2$ in $CO_2$ photoreduction, J. Catal., 221 (2004) 432–440.
[11] C.C. Wang, J.R. Li, X.L. Lv, Y.Q. Zhang, G.S. Guo, Photocatalytic organic pollutants degradation in metal-organic frameworks, Energy Environ. Sci., 7 (2014) 2831–2867.
[12] J.F. Tang, S. Chen, Y.P. Xu, W.J. Zhong, M. Ma, Z.J. Wang, Calibration and field performance of triolein embedded acetate membranes for passive sampling persistent organic pollutants in water, Environ. Pollut., 164 (2012) 158–163.
[13] R. Asahi, T. Morikawa, T. Ohwaki, K. Aoki, Y. Taga, Visible-light photocatalysis in nitrogen-doped titanium oxides, Science, 293 (2001) 269–271.
[14] T. Tong, J. Zhang, B. Tian, F. Chen, D. He, Preparation of $Fe^{3+}$-doped $TiO_2$ catalysts by controlled hydrolysis of titanium alkoxide and study on their photocatalytic activity for methyl orange degradation, J. Hazard. Mater., 155 (2008) 572–579.
[15] R. Buchel, S.E. Pratsinis, A. Baiker, Mono- and bimetallic Rh and Pt NSR-catalysts prepared by controlled deposition of noble metals on support or storage component, Appl. Catal., B, 113–114 (2012) 160–171.
[16] V. Celorrio, M.G. Montes de Oca, D. Plana, R. Moliner, D.J. Fermín, M.J. Lázaro, Electrochemical performance of Pd and Au-Pd core-shell nanoparticles on surface tailored carbon black as catalyst support, Int. J. Hydrogen Energy, 37 (2012) 7152–7160.
[17] Y. Wang, G.H. Chen, Q.H. Shen, F.M. Zhang, G.L. Chen, Hydrothermal synthesis and photocatalytic activity of combination of flowerlike $TiO_2$ and activated carbon fibers, Mater. Lett., 116 (2014) 27–30.
[18] X.W. Zhang, L.C. Lei, Preparation of photocatalytic $Fe_2O_3$–$TiO_2$ coatings in one step by metal organic chemical vapor deposition, Appl. Surf. Sci., 254 (2008) 2406–2412.
[19] H. Meng, W. Hou, X.X. Xu, J.L. Xu, X. Zhang, $TiO_2$-loaded activated carbon fiber: hydrothermal synthesis, adsorption properties and photocatalytic activity under visible light irradiation, Particuology, 14 (2014) 38–43.
[20] H.X. Huang, S.X. Chen, C. Yuan, Platinum nanoparticles supported on activated carbon fiber as catalyst for methanol oxidation, J. Power Sources, 175 (2008) 166–174.
[21] M.C. Macías-Pérez, M.A. Lillo-Ródenas, A. Bueno-López, $SO_2$ retention on CaO/activated carbon sorbents. Part II. Effect of the activated carbon support, Fuel, 87 (2008) 2544–2550.
[22] L. Zhang, Q. Zhou, J.Y. Liu, N. Chang, Phosphate adsorption on lanthanum hydroxide-doped activated carbon fiber, Chem. Eng. J., 6 (2012) 160–167.
[23] J.W. Shi, J.T. Zheng, P. Wu, Immobilization of $TiO_2$ films on activated carbon fiber and their photocatalytic degradation properties for dye compounds with different molecular size, Catal. Commun., 9 (2008) 1846–1850.
[24] S.H. Yao, J.Y. Li, Z.L. Shi, Immobilization of $TiO_2$ nanoparticles on activated carbon fiber and its photodegradation performance for organic pollutants, Particuology, 8 (2010) 272–278.
[25] W.X. Liu, J. Ma, X.G. Qu, Hydrothermal synthesis of (Fe, N) co-doped $TiO_2$ powders and their photocatalytic properties under visible light irradiation, Res. Chem. Intermed., 35 (2009) 321–328.
[26] L. Gomathi Devi, R. Kavitha, A review on plasmonic metal-$TiO_2$ composite for generation, trapping, storing and dynamic vectorial transfer of photogenerated electrons across the Schottky junction in a photocatalytic system, Appl. Surf. Sci., 360 (2016) 601–622.
[27] S. Larumbea, M. Mongeb, C. Gómez-Poloa. Comparative study of (N, Fe) doped $TiO_2$ photocatalysts, Appl. Surf. Sci., 327 (2015) 490–497.
[28] Y. Cong, J. Zhang, F. Chen, M. Anpo, D. He, Preparation, photocatalytic activity, and mechanism of nano-$TiO_2$ co-doped with nitrogen and iron (III), J. Phys. Chem. C, 111 (2007) 10618–10623.
[29] L.Q. Jing, H.G. Fu, B.Q. Wang, D.J. Wang, B.F. Xin, S.D. Li, J.Z. Sun, Effects of Sn dopant on the photoinduced charge property and photocatalytic activity of $TiO_2$ nanoparticles, Appl. Catal., B, 62 (2006) 282–291.
[30] Y.J. Liu, A.B. Wang, R. Claus, Molecular self-assembly of $TiO_2$/polymer nanocomposite films, J. Phys. Chem. B, 101 (1997) 1385–1388.
[31] Y. Zhang, W. Zhu, X. Cui, W. Yao, T. Duan, One-step hydrothermal synthesis of iron and nitrogen co-doped $TiO_2$ nanotubes with enhanced visible-light photocatalytic activity, CrystEngComm, 17 (2015) 8368–8376.
[32] H.H.H. Lin, A.Y.C. Lin, C.L. Hung, Photocatalytic oxidation of cytostatic drugs by microwave-treated N-doped $TiO_2$ under visible light, J. Chem. Technol. Biotechnol., 90 (2015) 1345–1354.
[33] T. Hirakawa, P.V. Kamat, Charge separation and catalytic activity of Ag@$TiO_2$ core-shell composite clusters under UV-irradiation, J. Am. Chem. Soc., 127 (2005) 3928–3934.
[34] B. Chi, L. Zhao, T. Jin, One-step template-free route for synthesis of mesoporous N-doped titania spheres, J. Phys. Chem. C, 111 (2007) 6189–6193.
[35] X.Y. Xu, X.S. Zhou, L.L. Zhang, L.M. Xu, L. Ma, J. Luo, M.J. Li, L.H. Zeng, Photoredox degradation of different water pollutants (MO, RhB, MB, and Cr(VI)) using Fe-N-S-tri-doped $TiO_2$ nanophotocatalyst prepared by novel chemical method, Mater. Res. Bull., 70 (2015) 106–113.
[36] W.R. Zhao, Y.J. Li, M. Zhang, J.S. Chen, L.H. Xie, Q.M. Shi, X. Zhu, Direct microwave-hydrothermal synthesis of Fe-doped titania with extended visible-light response and enhanced $H_2$-production performance, Chem. Eng. J., 283 (2016) 105–113.